FAUST: VIII. The protostellar disc of VLA 1623-2417W and its streamers imaged by ALMA

Mercimek, S.; Podio, L.; Codella, C.; Chahine, L.; López-Sepulcre, A.; Ohashi, S.; ... ; Yamamoto, S.

Monthly Notices of the ROYAL ASTRONOMICAL SOCIETY

MNRAS **522,** 2384–2392 (2023)
Advance Access publication 2023 April 11

https://doi.org/10.1093/mnras/stad964

FAUST – VIII. The protostellar disc of VLA 1623–2417W and its streamers imaged by ALMA

S. Mercimek,[1,2★] L. Podio,[1] C. Codella,[1,3] L. Chahine,[4,5] A. López-Sepulcre,[3,4] S. Ohashi,[6] L. Loinard,[7,8] D. Johnstone,[9,10] F. Menard,[3] N. Cuello,[3] P. Caselli,[11] J. Zamponi,[11] Y. Aikawa,[12] E. Bianchi,[1,13] G. Busquet,[14,15,16] J. E. Pineda,[11] M. Bouvier,[17] M. De Simone,[1,18] Y. Zhang,[6,19] N. Sakai,[6] C. J. Chandler,[20] C. Ceccarelli,[3] F. Alves,[11] A. Durán,[7] D. Fedele,[1] N. Murillo,[6] I. Jiménez-Serra[21] and S. Yamamoto[12,22]

Affiliations are listed at the end of the paper

Accepted 2023 March 28. Received 2023 March 28; in original form 2022 November 9

ABSTRACT

More than 50 per cent of solar-mass stars form in multiple systems. It is therefore crucial to investigate how multiplicity affects the star and planet formation processes at the protostellar stage. We report continuum and $C^{18}O$ (2–1) observations of the VLA 1623–2417 protostellar system at 50 au angular resolution as part of the ALMA (Atacama Large Millimeter/submillimeter Array) Large Program FAUST. The 1.3 mm continuum probes the discs of VLA 1623A, B, and W, and the circumbinary disc of the A1 + A2 binary. The $C^{18}O$ emission reveals, for the first time, the gas in the disc envelope of VLA 1623W. We estimate the dynamical mass of VLA 1623W, $M_{\rm dyn} = 0.45 \pm 0.08$ $M_\odot$, and the mass of its disc, $M_{\rm disc} \sim 6 \times 10^{-3}$ $M_\odot$. $C^{18}O$ also reveals streamers that extend up to 1000 au, spatially and kinematically connecting the envelope and outflow cavities of the A1 + A2 + B system with the disc of VLA 1623W. The presence of the streamers, as well as the spatial (∼1300 au) and velocity (∼2.2 km s^{-1}) offsets of VLA 1623W, suggests that either sources W and A + B formed in different cores, interacting between them, or source W has been ejected from the VLA 1623 multiple system during its formation. In the latter case, the streamers may funnel material from the envelope and cavities of VLA 1623AB on to VLA 1623W, thus concurring to set its final mass and chemical content.

Key words: ISM: kinematics and dynamics – ISM: molecules – stars: protostars – ISM: individual objects: VLA 1623–2417.

1 INTRODUCTION

Observational studies of solar-mass star-forming regions indicate a high fraction of multiplicity, ∼30–50 per cent (e.g. Duchêne et al. 2007; Chen et al. 2013; Tobin et al. 2016, 2022; Offner et al. 2022). It is therefore crucial to investigate what are the processes that lead to the formation of low-mass stars and their discs in multiple systems, in terms of dynamical interactions between protostars, ejection phenomena, and streamers stripping away or feeding gas and dust to the individual protostellar discs. Protostellar surveys (e.g. Reipurth 2000; Ward-Thompson et al. 2007; Chen et al. 2013; Tobin et al. 2016) indicate that the multiplicity fraction (MF) is higher during the Class 0 stage (sources with age ∼10^4 yr, MF up to 0.5–0.8), with respect to later Class I and Class II sources (age >10^5 yr, MF of 0.2–0.3). This lowering MF with time may be due to dynamical interactions that cause the ejection of one component from the protostellar system (Reipurth 2000; Sadavoy & Stahler 2017). Moreover, recent interferometric observations reveal the presence of accretion streamers in protostellar systems spanning sizes from 1000 au (e.g. Takakuwa et al. 2017; Alves et al. 2019; Hull et al. 2020; Pineda et al. 2022) up to 10^4 au (e.g. Pineda et al. 2020; Murillo et al. 2022). Such accretion streamers are also observed at more evolved Class I/II stages and may play a crucial role in determining the final disc mass and chemical composition (Liu et al. 2016; Akiyama et al. 2019; Garufi et al. 2022; Valdivia-Mena et al. 2022).

The VLA 1623–2417 region (VLA 1623 hereafter) is an archetypical laboratory to investigate low-mass star formation within a multiple protostellar system and the associated phenomena: ejection, accretion, and dynamical interactions between sources (Murillo et al. 2013; Harris et al. 2018; Hara et al. 2021; Ohashi et al. 2022). VLA 1623 is located in Ophiuchus A at a distance, *d*, of 131 pc (Gagné et al. 2018), and consists of four protostellar sources: VLA 1623A, a close Class 0 binary, with separation between the components (A1 and A2) of ∼30 au, surrounded by a circumbinary disc; VLA 1623B, a Class 0 protostar located ∼130 au west of VLA 1623A and associated with an edge-on disc; and VLA 1623W, classified as a Class I protostar and located ∼1300 au west of the A binary, also associated with an edge-on disc (e.g. Bontemps & Andre 1997; Murillo & Lai 2013; Harris et al. 2018; Kawabe et al. 2018).

The A1, A2, and B protostellar sources drive high-velocity outflows along the NW–SE direction detected in CO and H_2 (e.g. Andre et al. 1990; Caratti o Garatti et al. 2006; Santangelo et al. 2015; Hara et al. 2021). The outflows open low-velocity wide-angle cavities observed in CCH and CS (e.g. Ohashi et al. 2022). Emission in SO and $C^{18}O$ also probes accretion flows towards the circumbinary

★ E-mail: seymamercimek@gmail.com

disc of VLA 1623A (Hsieh et al. 2020). The outflow cavities rotate coherently with the dense parental envelope (Ohashi et al. 2022). On the other hand, the disc of VLA 1623B counter-rotates with respect to the envelope and outflow cavities, and the A1, A2, and B discs are misaligned, suggesting that the system is dynamically unstable (Hara et al. 2021; Codella et al. 2022; Ohashi et al. 2022).

The nature of the more distant component of the cluster, VLA 1623W, located ∼1300 au away from VLA 1623A and B, and its associated phenomena are only poorly characterized. Maury, Ohashi & André (2012) suggested that W could be a shocked cloudlet produced by the outflow driven by VLA 1623A. ALMA continuum images, however, revealed that W is a protostar with an edge-on disc (Harris et al. 2018; Sadavoy et al. 2019; Michel et al. 2022). Based on the analysis of the spectral energy distribution, Murillo et al. (2018) classified VLA 1623W as a Class I protostar, due to the four times lower luminosity and 20 times lower envelope mass compared to VLA 1623A and B. Observations of $C^{18}O$ (2–1) line emission by Murillo et al. (2013) suggest that the systemic velocity of VLA 1623W is between 0 and 1 km s^{-1}, which differs from VLA 1623A's systemic velocity (+3.8 km s^{-1}; Ohashi et al. 2022). Murillo et al. (2013) and Harris et al. (2018) suggest that VLA 1623W may have been ejected from the system composed of A1, A2, and B. In this paper, we report ALMA observations of $C^{18}O$ (2–1) and continuum emission at 1.3 mm used to investigate the gas in the disc of VLA 1623W and the source dynamical interaction with the other protostellar sources in the VLA 1623 multiple protostellar system.

2 OBSERVATIONS AND DATA REDUCTION

The VLA 1623 protostellar system was observed between October 2018 and March 2020 as part of the ALMA Large Program FAUST (Fifty AU STudy of the chemistry in the disc/envelope system of solar-like protostars; 2018.1.01205.L, PI: S. Yamamoto; Codella et al. 2022). We observed in the Band 6 frequency range 216–234 GHz, using the 12-m array (C43-4 and C43-1) and 7-m array of the Atacama Compact Array. The observations were centred at $\alpha_{2000} = 16^{h}26^{m}26\overset{s}{.}392$, $\delta_{2000} = -24°24'30\overset{''}{.}69$. The $C^{18}O$ (2–1) line at 219 560.3 MHz (E_{up} = 16 K; Müller et al. 2005) is covered by a narrow spectral window with a bandwidth of 62.5 MHz (87 km s^{-1}) and a channel width of 122 kHz (0.17 km s^{-1}). A spectral window with a bandwidth of 1825 MHz and a channel width of 977 kHz (1.25 km s^{-1}) has been used to image the continuum emission.

We used the Common Astronomy Software Applications (CASA) package 5.6.1-8 version (McMullin et al. 2007) to obtain the calibrated visibilities, and 6.2.1 version to obtain and to image a clean data. The multiscale deconvolver was used (Cornwell 2008; Rau & Cornwell 2011). In addition to the standard pipelines, an additional calibration routine (http://www.aoc.nrao.edu/~gmoellen/; Moellenbrock et al., in preparation) has been used to correct for T_{sys} and for spectral data normalization. We used line-free frequencies to recover the continuum emission for each configuration and perform self-calibration. The correction of the complex gain has been derived from the self-calibration and spontaneously carried out to line visibilities of the data. Following that, to produce continuum-subtracted line data we subtracted the continuum model, derived from the self-calibration. Also, the phase self-calibration technique along with long solution interval amplitudes has been used to align positions across all configurations. The task *tclean* was used to obtain the image of the continuum and the datacube of the molecular emission. We adopted Briggs weighting with a robustness parameter of −2.0 (uniform weighting) for the continuum to obtain the highest angular resolution (beam: 0.42 arcsec × 0.32 arcsec, PA = −65°). On the other hand, a robustness parameter of 0.5 was employed for the molecular emission to optimize the signal-to-noise ratio, consistent with the previous FAUST paper on VLA 1623 (Ohashi et al. 2022). Finally, we applied primary beam corrections.

The data analysis was carried out using the IRAM-GILDAS[1] software package. We produced two continuum-subtracted $C^{18}O$ (2–1) datacubes: (1) combining only the data taken with the 12-m array to sample small-scale structures (beam: 0.48 arcsec × 0.40 arcsec, PA = −82°; θ_{MRS} ∼ 14 arcsec, corresponding to ∼1800 au; see Figs 3 and A1 and panels c and d of Fig. 4); and (2) combining the data taken with the 12- and 7-m arrays to recover emission extending up to ∼3000 au (beam: 0.53 arcsec × 0.44 arcsec, PA = −74°, θ_{MRS} ∼ 24 arcsec, corresponding to ∼3150 au; used in Figs 1 and 2 and panels a and b of Fig. 4). The noise root mean square (rms) is 1.8 and 1.4 mJy per beam per channel for $C^{18}O$ datacubes (1) and (2), respectively. The rms of the continuum map is 0.26 mJy per beam.

3 RESULTS

3.1 Continuum emission at 1.3 mm

Fig. 1 shows the map of the 1.3 mm continuum emission (black contours), obtained combining the 12-m and 7-m data. The protostellar sources A, B, and W are detected, as well as the circumbinary disc, but the angular resolution is too low to disentangle the close binary components, A1 and A2, resolved by Harris et al. (2018) at 0.9 mm (separation ∼30 au). We fit the continuum emission towards VLA 1623A, B, and W with the CASA task *imfit*, which performs a two-dimensional elliptical Gaussian fit. The obtained coordinates of the continuum peak (RA_{J2000}, $Dec._{J2000}$), the ellipse size, the position angle, the integrated intensity at 1.3 mm ($F_{1.3\,mm}$), and the peak intensity are reported in Table 1. The results of the fit are in agreement with those obtained by Harris et al. (2018) at 0.9 mm. For source W, we find that the disc is almost edge-on (inclination $i \simeq 80°$), and has a diameter of ∼93 au. From the integrated intensity at 1.3 mm, we estimate the mass of dust in the discs, M_{dust}, as (Hildebrand 1983; Beckwith et al. 1990)

$$M_{dust} = \frac{F_{1.3\,mm} d^2}{\kappa_\nu B_\nu (T_{dust})}. \quad (1)$$

We assume isothermal conditions and optically thin emission, dust opacity (κ_ν) at 1.3 mm of 2.17 cm^2 g^{-1} (Zamponi et al., submitted), and dust temperature, T_{dust}, between 20 K, the typical value assumed for Class II discs (e.g. Beckwith et al. 1990), and 50 K, to account for possible warmer dust in Class 0 and I discs (e.g. Zamponi et al. 2021). Table 1 reports the derived M_{dust} values towards source A, source B, and source W.

For source W, assuming a gas-to-dust ratio of 100, we obtain a total disc mass of $6 \pm 3 \times 10^{-3}$ $M_\odot$. The difference with the estimate obtained by Sadavoy et al. (2019) in the same ALMA band (1×10^{-2} $M_\odot$) is due to the 10 per cent uncertainty on the flux calibration and the different assumed distance, dust opacity, and temperature. Moreover, the derived disc mass is affected by large uncertainty due to: (i) the assumption on the gas-to-dust ratio. If this is lower than 100 (e.g. Ansdell et al. 2016), the estimated disc mass should be regarded as an upper limit; and (ii) the assumption that the dust continuum emission is optically thin. If the emission is optically thick, the estimated disc mass is a lower limit.

[1] http://www.iram.fr/IRAMFR/GILDAS

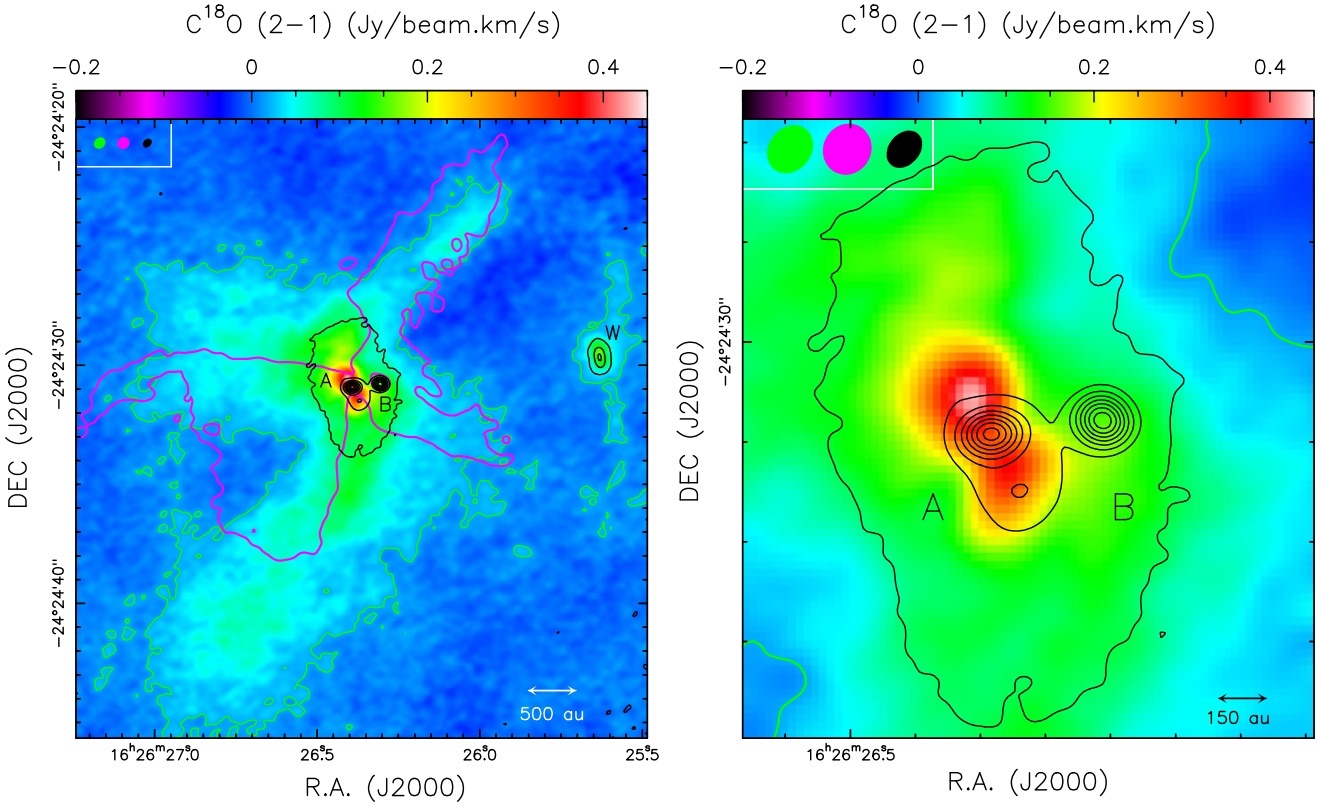

Figure 1. *Left:* The VLA 1623–2417 system: integrated intensity map (moment 0) of $C^{18}O$ (2–1) (colour scale) by overlaying the dust continuum emission at 1.3 mm (black contour). The 12-m + 7-m data set has been used. The positions of the A, B, and W protostars are labelled. The $C^{18}O$ emission is integrated from −6.0 to +10.0 km s^{-1}. The black continuum contours start from 3σ (0.78 mJy per beam) with intervals of 40σ. The green contour is for the 3σ level (18 mJy km s^{-1} per beam) of the $C^{18}O$ moment 0 map. The magenta thick contour is the CS(5–4) emission (25σ) that traces the outflow cavity walls associated with VLA 1623A (from Ohashi et al. 2022). The synthesized beams (upper left corner) are drawn in green, magenta, and black for the $C^{18}O$, CS, and the dust continuum emission, respectively (Section 2). *Right:* Zoom-in of the moment 0 map towards sources A and B.

3.2 $C^{18}O$ (2–1) emission

Fig. 1 shows the velocity-integrated intensity map (moment 0) of $C^{18}O$ (2–1) towards the VLA 1623 protostellar system (colour scale) by overlaying the dust continuum emission at 1.3 mm (black contour) to pinpoint the positions of the protostellar sources A, B, and W, and of the circumbinary disc around the A1 + A2 binary system (Harris et al. 2018). The magenta contour indicates the 25σ level of the CS(5–4) emission integrated on the velocity interval 3.4–4.2 km s^{-1}, which probes the outflow cavity walls associated with VLA 1623A (from Ohashi et al. 2022). The $C^{18}O$ emission probes the circumbinary disc and the envelope around the A1 + A2 binary system and the outflow cavity walls first identified through CS (5–4) emission (Ohashi et al. 2022). $C^{18}O$ (2–1) also traces a bright elongated structure south of the circumbinary disc. Moreover, $C^{18}O$ shows emission towards the VLA 1623W disc continuum, as well as an elongated structure to the north and to the south of W, roughly along the disc position angle. This elongated emission cannot be due to a jet or an outflow as it is not perpendicular to the disc PA.

To analyse the spatial distribution and kinematics of the different emitting components, we examine the channel maps of $C^{18}O$ (see Figs 2 and 3). At low velocities, i.e. between +0.2 and +3.0 km s^{-1}, $C^{18}O$ emission extends on large scales (> 2 arcsec from the continuum peak of VLA 1623W) and shows arc-like structures (hereafter called streamers) that elongate up to > 1000 au distances from VLA 1623W connecting with the emission detected towards VLA 1623A and B (Fig. 2). The spatio-kinematical properties and the origin of the $C^{18}O$ low-velocity emission are discussed in Section 3.2.2. In contrast, the emission at high velocities, i.e. between −2.6 and −0.4 km s^{-1}, and +3.6 and +5.8 km s^{-1}, is compact (<1 arcsec from the VLA 1623W continuum peak) and shows a velocity gradient along the PA of the dusty disc (Fig. 3). This compact high-velocity emission probes the molecular gas in the disc of VLA 1623W and is discussed next, in Section 3.2.1.

3.2.1 The gas towards the disc of VLA 1623W

Fig. 4 (panels c and d) shows the moment 0 and moment 1 maps of $C^{18}O$ (2–1) emission towards VLA 1623W integrated up to high velocities (from –2.6 to +5.8 km s^{-1}). In this case, only the combined 12-m array is used to minimize contamination from the large-scale emission. The continuum emission at 1.3 mm is shown by black contours. A velocity gradient along the disc PA (as derived from the continuum fit, $PA_{disc} \sim 10°$) is observed at an ∼50-au scale. The moment 1 map indicates that the systemic velocity of VLA 1623W is $V_{sys}(W) \simeq +1.6$ km s^{-1}, as it corresponds to the central velocity of the range where compact blueshifted and redshifted emission is detected and to the mean velocity at the peak continuum emission. In agreement with Murillo et al. (2013), our $C^{18}O$ map indicates that the systemic velocity of VLA 1623W is different from that of VLA 1623A and B (+3.8 km s^{-1}; Ohashi et al. 2022). The channel maps in Fig. 3 complement the information on the gas kinematics towards the disc of VLA 1623W, showing the high-velocity emission

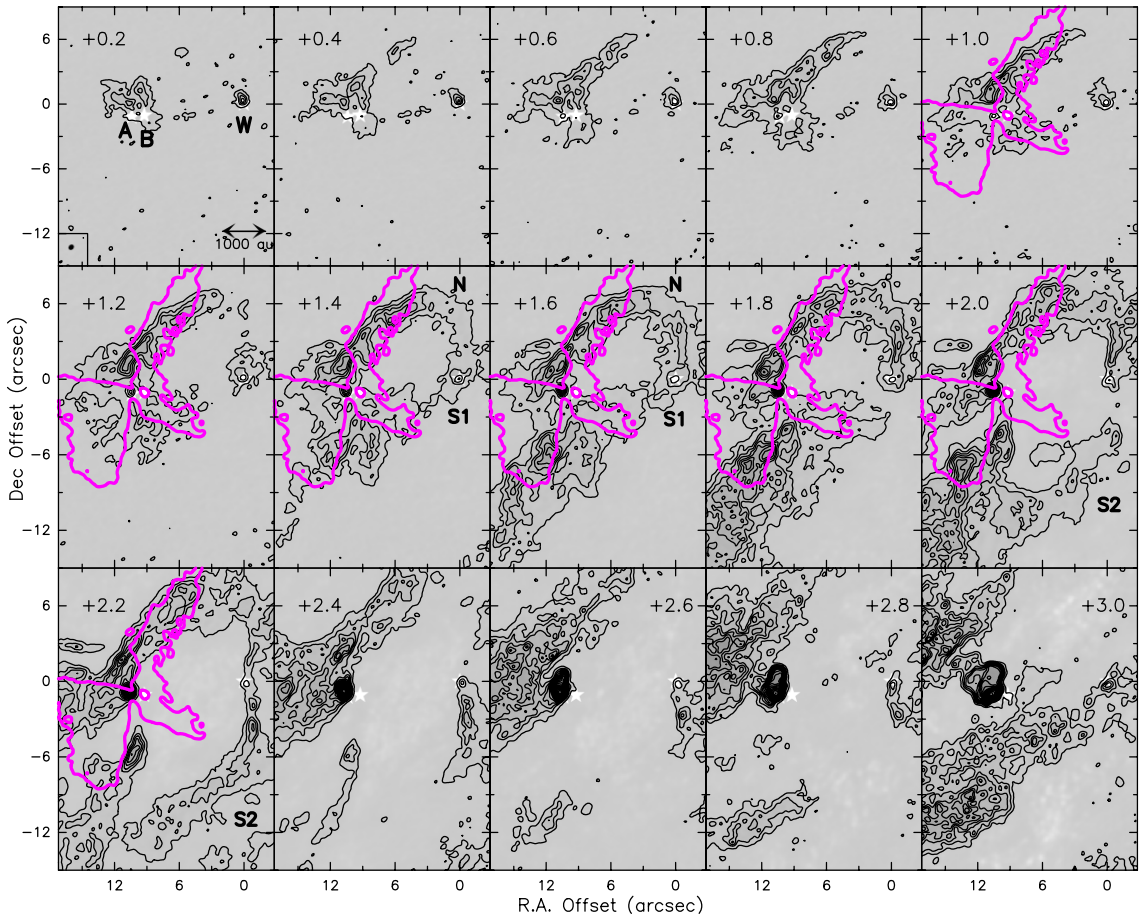

Figure 2. Channel maps of the $C^{18}O$ (2–1) emission on the low velocity range ([+0.2, +3.0] km s^{-1}). The first contour is at 3σ (4.2 mJy per beam) and the step is 10σ. The synthesized beam is shown by the black ellipse in the bottom left corner of the first channel (beam: 0.53 arcsec × 0.44 arcsec). The positions of VLA 1623A, B, and W are indicated by the white stars and are labelled in the first channel. The magenta contours in the channels from +1.0 to +2.2 km s^{-1} indicate the outflow cavity walls probed by CS (5–4) emission (25σ contour, from Ohashi et al. 2022). The northern, N, and southern, S1 and S2, streamers are labelled.

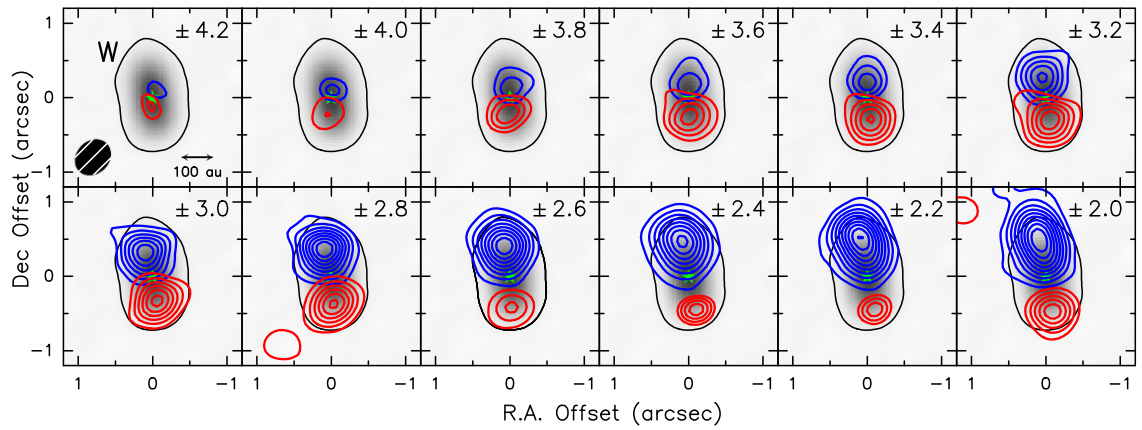

Figure 3. Channel maps of the $C^{18}O$ (2–1) compact emission around the VLA 1623W protostar (green star) at high redshifted and blueshifted velocities, i.e. from ±2 to ±4.2 km s^{-1} with respect to the VLA 1623W systemic velocity (+1.6 km s^{-1}). First contours and steps are 3σ (5.4 mJy per beam). The velocity offset with respect to V_{sys}(W) is reported in the top right corner of each panel. The black contour is the 3σ level of the 1.3 mm continuum emission, which is also shown by the greyscale background. The synthesized beam (0.48 arcsec × 0.40 arcsec) is shown in the bottom left corner of the first channel.

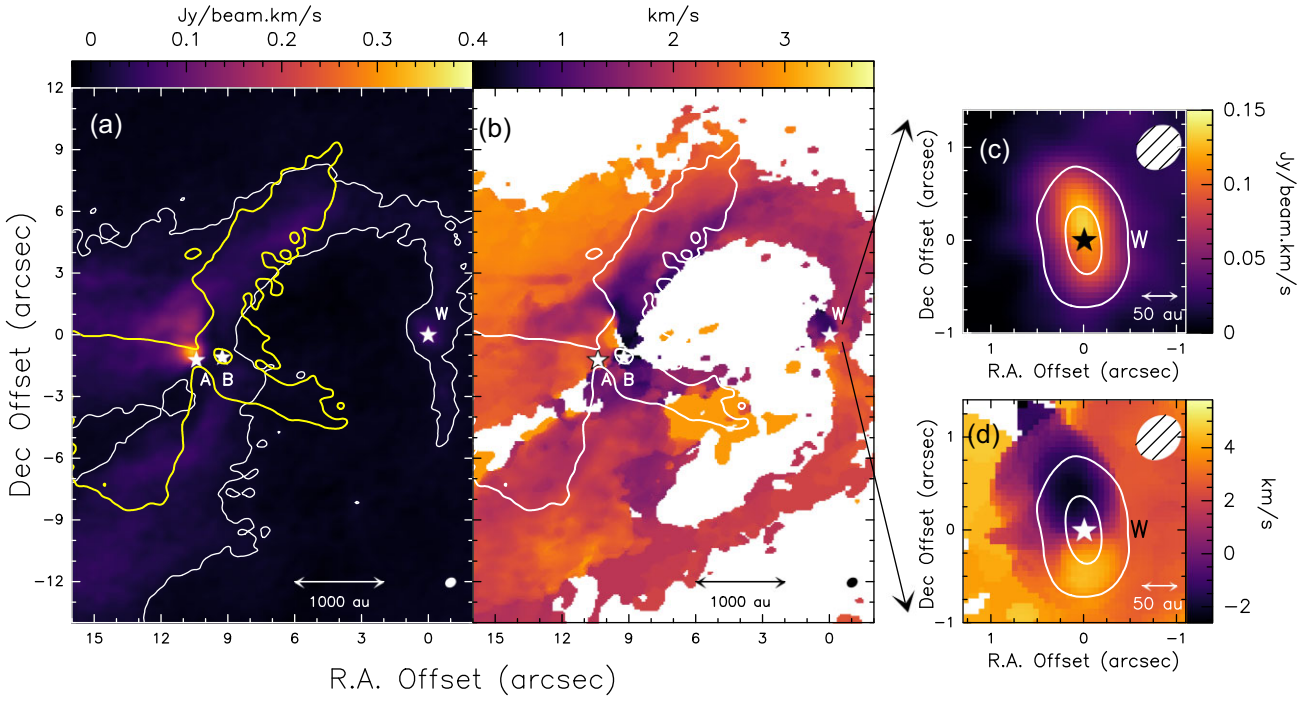

Figure 4. Integrated intensity (moment 0) and intensity-weighted mean velocity (moment 1) maps of $C^{18}O$ (2–1) towards VLA 1623–2417. The RA and Dec. offsets are with respect to the position of VLA 1623W. *Panels a and b*: Moment 0 and 1 maps over the low velocity range ([+0.2, +3.0] km s^{-1}). The white stars indicate the A, B, and W protostars, the white contour in panel a indicates the 3σ emission (9 mJy km s^{-1} per beam), the ellipse shows the synthesized beam (0.53 arcsec × 0.44 arcsec), and the yellow in panel a and the white contour in panel b reveal the 25σ CS (5–4) emission probing the cavity outflow walls associated with VLA 1623A (from Ohashi et al. 2022). *Panels c and d*: Moment 0 and moment 1 maps of VLA 1623W over the high velocity range ([–2.6, +5.8] km s^{-1}). Continuum emission at 1.3 mm is shown by the white contours. The black and white stars indicate the position of VLA 1623W, and the white ellipse indicates the synthesized beam (0.48 arcsec × 0.40 arcsec).

Table 1. Peak coordinates, ellipse size, position angle, integrated and peak intensity of the continuum emission at 1.3 mm towards sources A1 + A2, B, and W.

Source	RA_{J2000} (^{hms})	$Dec._{J2000}$ ($^{\circ\prime\prime\prime}$)	Ellipse size ($'' \times ''$)	Position angle ($^\circ$)	$F_{1.3\,mm}$ (mJy)	Peak I (mJy per beam)	M_{dust}[a] (10^{-4} $M_\odot$)
A1 + A2	16:26:26.3907 ± 0.0013	–24.24.30.934 ± 0.017	0.49 (±0.01) × 0.33 (±0.01)	74 ± 20	158 ± 14	71 ± 4	1.6 ± 0.8
B	16:26:26.3063 ± 0.0001	–24.24.30.787 ± 0.002	0.32 (±0.04) × 0.16 (±0.03)	43 ± 5	121 ± 2	80 ± 1	1.2 ± 0.6
W	16:26:25.6312 ± 0.0002	–24:24:29.669 ± 0.005	0.71 (±0.01) × 0.12 (±0.02)	10.0 ± 0.8	59 ± 1	23.7 ± 0.3	0.6 ± 0.3

[a]The dust mass, M_{dust}, is derived from the integrated intensity assuming a dust temperature of 20–50 K.

at symmetric blueshifted and redshifted velocities with respect to V_{sys}(W) [from ($V_{LSR} - V_{sys}$) $\simeq \pm 2$ km s^{-1} to ($V_{LSR} - V_{sys}$) $\simeq \pm 4.2$ km s^{-1}]. The channel maps of the emission at lower velocity, i.e. from V_{sys} to ± 1.8 km s^{-1} with respect to systemic, are shown in the appendix (Fig. A1), and show that at low velocities the kinematics of the gas in the disc is contaminated by emission from the streamers mapped on larger scales in Fig. 2 and panels a and b of Fig. 4. In the channel maps at high velocities, instead, the peaks of the blueshifted and redshifted emission are located along the disc major axis, and the emission is more compact and peaks at smaller distances for increasing velocities with respect to V_{sys}(W) as expected in a Keplerian rotating disc.

The previous molecular line study towards VLA 1623W (Murillo et al. 2013) showed only $C^{18}O$ (2–1) blueshifted emission towards the northern disc side, plausibly due to lower sensitivity. Indeed, we find that the blueshifted disc side is brighter than the redshifted one up to velocities of ± 2.6 km s^{-1} with respect to systemic, likely due to contamination from the extended streamers observed at larger scales (see Section 3.2.2). At higher velocities, the emission from each disc side is symmetric. We therefore use the emission in the channels at radial velocities of ± 2.8 and ± 3.0 km s^{-1} to derive an estimate of the VLA 1623W dynamical mass, M_{dyn}. The emission in these channels peaks at a radial distance of 0.37 and 0.33 arcsec. By assuming Keplerian motion, we estimate a dynamical mass

$$M_{dyn} = r\frac{V^2}{G}, \quad (2)$$

where r and V are the distance and velocity of the blueshifted and redshifted peaks, respectively, deprojected for the disc inclination of 80°. The estimated dynamical mass is 0.45 ± 0.08 $M_\odot$.

The discovery of molecular emission towards the edge-on source W makes it a good candidate to investigate the gas vertical structure on scales <50 au, as recently performed for highly inclined protoplanetary discs by Louvet et al. (2018), Podio et al. (2020), and Teague et al. (2020). This is key to investigate the chemical composition of the disc in the region where planets are expected to form.

3.2.2 The streamers connecting VLA 1623W with the A + B system

Fig. 2 shows the channel maps of $C^{18}O$ (2–1) emission at low velocities, i.e. between +0.2 and +3.0 km s^{-1}. Three streamers connecting VLA 1623A and B with VLA 1623W are observed: one in the northern VLA 1623 region, labelled as N, and the other two in the southern region labelled as S1 and S2 and detected on velocities of [+1.2, +1.8] and [+2.0, +2.8] km s^{-1}, respectively. Fig. 4 shows the moment 0 (panel a) and moment 1 (panel b) maps obtained for the low velocity range ([+0.2, +3.0] km s^{-1}). Both figures use the 12-m + 7-m data set. The northern streamer partially overlaps with the north-west blueshifted cavity wall opened by the outflow(s) driven by VLA 1623A (see the yellow/white contours, from Ohashi et al. 2022). At distances from VLA 1623A larger than ∼1000 au, the molecular emission bends towards the south until it connects to the northern side of the VLA 1623W disc. In the southern region, the streamer S1 overlaps with the south-west cavity wall opened by the outflow(s) driven by VLA 1623A. The streamer S2, on the other hand, connects the envelope surrounding VLA 1623A and B with the southern side of the VLA 1623W disc extending towards the south. In summary, the S1 and S2 streamers have both different spatial distribution and different velocities; therefore, they are labelled as different streamers.

The velocities of the observed streamers are consistent with those of the outflow cavities and the envelope probed by CS(5–4) and $H^{13}CO^+$ emission by Ohashi et al. (2022; see their figs 12, 13, and 16), and with the velocities of the VLA 1623W disc: the blueshifted outflow cavity/streamer north of VLA 1623A connects with the northern blueshifted side of the VLA 1623W edge-on disc, while the redshifted outflow cavity/streamer south of VLA 1623A connects with the southern redshifted side of the VLA 1623W disc. This indicates that the protostellar sources A and W are kinematically linked. In addition, the moment 1 map of $C^{18}O$ shows a velocity gradient along the southern streamer having larger redshifted velocities (by ∼1 km s^{-1}) at the connection with the VLA 1623W disc with respect to the portion of streamer connected with the VLA 1623A + B envelope. On the contrary, no clear velocity gradient is observed along the northern streamer. The lack of a velocity gradient along the northern streamer may indicate that the gas motion occurs in the plane of the sky (Alves et al. 2020).

4 DISCUSSION: ON THE ORIGIN OF VLA 1623W

The FAUST ALMA observations of the multiple system VLA 1623 reveal for the first time the gas kinematics towards the more distant component, VLA 1623W. Specifically, $C^{18}O$ (2–1) emission probes the following structures: (i) the molecular gas in the disc of VLA 1623W with Keplerian motion on 50–100 au scales, constraining the protostellar mass ($M_{\rm dyn}$ ∼ 0.45 $M_\odot$); and (ii) streamers that extend on scales >1000 au and connect spatially and kinematically the two sides of the edge-on disc of VLA 1623W ($PA_{\rm disc}$ ∼ 10°, i ∼ 80°, $M_{\rm disc}$ ∼ 6 × 10^{-3} $M_\odot$) with the envelope associated with VLA 1623A and B.

Molecular streamers have been observed in other multiple systems, e.g. between the components of IRAS 16293−2422 separated by a distance of ≃400 au (Pineda et al. 2012; Jacobsen et al. 2018; van der Wiel et al. 2019; Murillo et al. 2022). In the case of VLA 1623, however, the large spatial (∼1300 au) and kinematic (∼2.2 km s^{-1}) offsets between VLA 1623AB and VLA 1623W suggest that VLA 1623W does not belong to the same molecular core as VLA 1623AB. On the other hand, the molecular streamers connecting the disc of VLA 1623W with the envelope/cavities of VLA 1623A and VLA 1623B suggest that VLA 1623W is not a background or foreground object. In this context, there are two possible scenarios: (1) VLA 1623W has formed in a core that is close by and gravitationally interacting with the envelope of VLA 1623AB; and (2) VLA 1623W was ejected from the multiple system composed of A1, A2, and B due to dynamical interactions during the system's formation, as first proposed by Murillo et al. (2013).

4.1 Hypothesis 1: formation in a separate core

In the first scenario, the observed streamers are produced by the interaction of multiple cores in the Ophiuchus A star-forming region hosting the VLA 1623A, B and W protostars. Chen & Hirano (2018) mapped Ophiuchus A at a spatial resolution ≥5 arcsec to investigate the physical and chemical properties of the region in continuum and molecular lines by combining interferometric (SMA) and single-dish (IRAM-30m) data. The maps show that Ophiuchus A consists of three ridges aligned along the north–south direction and that VLA 1623A + B and VLA 1623W are located in adjacent ridges (see figs 1 and 4 by Chen & Hirano 2018). Therefore, the streamers probed by $C^{18}O$ (2–1) that connect VLA 1623A + B with VLA 1623W could be the signature of the gravitational pull across adjacent ridges. However, the maps by Chen & Hirano (2018) indicate that the systemic velocities of the two adjacent ridges are similar (both being between +3 and +4 km s^{-1}), while our observations indicate that VLA 1623W has a systemic velocity of +1.6 km s^{-1}, which differs from the systemic velocity of VLA 1623AB (+3.8 km s^{-1}) and the two ridges. Thus, this first scenario is unlikely.

4.2 Hypothesis 2: ejection or fly-by

In the second scenario, the protostellar source VLA 1623W formed in the same envelope as VLA 1623A and B, and has been later ejected from the multiple system due to a close interaction (Murillo et al. 2013). According to Harris et al. (2018), the later evolutionary stage of VLA 1623W (Class I) could be due to the loss of most of its original parental envelope during the ejection. The ejection scenario is further supported by the kinematics of the system. The ratio between the kinematical and the gravitational energy of the system composed of A, B, and W (protostellar masses of 0.4, 1.7, and 0.45 $M_\odot$, envelope masses of 0.8, 0.2, and 0.04 $M_\odot$) is ≃1, which indicates that the system is likely unstable (Pineda et al. 2015). Other signatures of instability are as follows: (i) the axis of the circumbinary disc around the A1 + A2 binary is misaligned by 12° with respect to both the large-scale outflow and the rotation axis of the molecular envelope (Ohashi et al. 2022); (ii) the edge-on disc of VLA 1623B counter-rotates with respect to the outflow driven by VLA 1623A and the surrounding envelope; and (iii) the circumstellar discs of A1 and A2 have inclinations that may differ by ∼70° based on the orientation of the high-velocity outflows (Harris et al. 2018; Murillo et al. 2018; Codella et al. 2022; Ohashi et al. 2022). Given the high dynamic instability, all of the protostars in the system might have been bound at the time of their formation, with one or more components later ejected due to a close encounter (e.g. Reipurth & Mikkola 2012; Pineda et al. 2015).

In the ejection scenario, the velocity gradient of 1 km s^{-1} detected along the southern streamer indicates either material falling on VLA 1623W if the streamer is located in front (i.e. between W and the observer) or alternatively gas moving away from VLA 1623W towards A + B if the streamer is located on the other side of W. Note that the close encounter that occurs during the ejection of one of the members of a multiple stellar system has a similar dynamical effect to that of a stellar fly-by (Cuello, Ménard & Price 2023). In the case

Table 2. The offset (in arcsec) in δRA and δDec., and the resulting separation (ρ) between sources A and W and between sources B and W at the epochs of the VLA-X observations (1991.8) and the ALMA Band 6 observations (2019.5).

	Offset between A and W		Offset between B and W	
	VLA-X 1991.8	ALMA-B6 2019.5	VLA-X 1991.8	ALMA-B6 2019.5
δRA	-10.56 ± 0.03 arcsec	-10.383 ± 0.003 arcsec	-9.37 ± 0.02 arcsec	-9.218 ± 0.001 arcsec
δDec.	$+1.39 \pm 0.03$ arcsec	$+1.260 \pm 0.003$ arcsec	$+1.39 \pm 0.03$ arcsec	$+1.120 \pm 0.002$ arcsec
ρ	10.65 ± 0.06 arcsec	10.46 ± 0.02 arcsec	9.44 ± 0.05 arcsec	9.29 ± 0.01 arcsec

of a fly-by, if the outer perturber, VLA 1623W, follows a prograde orbit near the disc envelope of A + B, this could lead to the formation of streamers like the ones observed in $C^{18}O$ (e.g. UX Tau; Ménard et al. 2020; Zapata et al. 2020; Dong et al. 2022). It is, however, puzzling that in VLA 1623 both streamers appear to point towards VLA 1623W since tidal perturbations of the disc typically trigger the formation of two diametrically opposed streamers, pointing in opposite directions (Clarke & Pringle 1993; Pfalzner 2003; Cuello et al. 2020). Interestingly, in the moment 0 maps in Figs 1 and 4 we tentatively detect a spiral arm south to VLA 1623AB that is diametrically opposed with respect to the northern spiral arm, N, which connect AB with W. If so, this would indicate that W and AB interacted recently, forming the diametrically opposed spiral arms during the encounter. In this scenario, the two southern arcs detected in the moment 1 map (S1 and S2) would not be associated with the encounter between W and the AB system. More in general, assuming that at least one of the streamers was produced by the dynamical interaction during the ejection of VLA 1623W, then the streamers' misalignment with respect to the discs' planes can be due to the fact that misaligned stellar fly-bys are more likely than coplanar ones (Bate 2018; Cuello et al. 2019).

We stress that both the ejection of a member in young multiple systems and stellar fly-bys are very common processes. In both cases, the expected velocities and eccentricities may cover a broad range of values (e.g. Cuello et al. 2023); therefore, to first order, fly-bys and ejections leave similar signatures. To distinguish between the two scenarios would require observations at different epochs and accurate astrometry and radial velocity measurements in order to reconstruct the orbit.

4.3 Proper motions between 1991.8 and 2019.5

In order to test the ejection scenario, we estimate the proper motions of VLA 1623W with respect to VLA 1623A and B by combining our FAUST ALMA Band 6 observations of the continuum at 1.3 mm, taken in 2019, with the data at 3.6 cm, taken with the VLA in the *X* band in 1991 (Andre, Ward-Thompson & Barsony 1993; project AB817). We measured the separation between A and W, and between B and W, in the VLA-X (1991.8) and ALMA-B6 (2019.5) images, which are separated by 27.7 yr. Table 2 reports the offset (in arcsec) in right ascension (δRA) and declination (δDec.) and the resulting separation (ρ) between source A and source W and between source B and source W at the two epochs.

From these values, the velocities on the plane of the sky between the sources can be derived. Namely, the velocity on the plane of the sky of A with respect to W is -4.4 ± 1.47 km s^{-1}, while that of B with respect to W is -3.5 ± 1.26 km s^{-1}. These measurements are in agreement with the proper motions estimated by Harris et al. (2018) based on ALMA observations taken in 2013 (Murillo et al. 2013) and 2016 but are affected by a lower uncertainty given the larger distance between the two epochs. Based on the above estimates, there is no significant difference in tangential velocity between VLA 1623W and A (or B) at the 3σ level. However, in the ejection scenario the velocity needed for VLA 1623W to move away from A + B up to a distance of ∼10 arcsec in 10^4 yr (i.e. the typical Class 0 age) is only 0.65 km s^{-1}, i.e. below the uncertainty associated with our proper motion measurements (∼1.3–1.5 km s^{-1}). Thus, the ejection scenario can be neither ruled out nor confirmed by the available proper motion.

5 CONCLUSIONS

We report observations of the continuum at 1.3 mm and $C^{18}O$ (2–1) line emission towards the multiple protostellar system VLA 1623–2417. We reveal for the first time the gas associated with the edge-on disc of VLA 1623W. From the gas kinematics, assuming Keplerian rotation, we estimate the source dynamical mass ($M_* = 0.45 \pm 0.08$ M$_\odot$). Moreover, we reveal three streamers connecting VLA 1623W with the VLA 1623A + B system. The spatial (∼1300 au) and velocity (∼2.2 km s^{-1}) offsets of VLA 1623W with respect to A + B, and its later evolutionary stage (Class I), suggest that either sources W and A + B formed in different cores or source W has been ejected from the multiple system during its formation, due to the interaction with one of its member. The available data on proper motions cannot confirm or rule out either of the two scenarios. Additional kinematical constraints are required in order to test the stellar encounter scenario for VLA 1623. In addition, observations of shock tracers, such as SO and SiO, at a spatial resolution of ∼10 au will allow for verification that the observed streamers are feeding the disc of VLA 1623W or that vice versa they funnel material from W to A and B. Such observations are required to assess the importance of streamers for disc formation and evolution.

ACKNOWLEDGEMENTS

This project has received funding from the EC H2020 research and innovation programme for (i) the project 'Astro-Chemical Origins' (ACO; No. 811312), (ii) the European Research Council (ERC) project 'The Dawn of Organic Chemistry' (DOC; No. 741002), and (iii) the ERC project Stellar Multiplicity on planet formation Across Disc Evolution (Stellar-MADE; No. 101042275). This study was also supported by grants-in-aid from the Ministry of Education, Culture, Sports, Science and Technology of Japan (18H05222, 19H05069, 19K14753, and 21K13954), by the Spanish Ministry of Science and Innovation/State Agency of Research MCIN/AEI/10.13039/501100011033 (PID2019-105552RB-C41), 'ERDF: a way of making Europe', by the Direccion General de Asuntos del Personal Academica Programa de Apoyo a Proyectos de Investigación e Innovación Tecnológica (DGAPA PAPIIT grants IN112417 and IN112820), Consejo Nacional de Ciencia y Tecnología-Agencia Espacial Mexicana (CONACYT-AEM grant 275201, and CONACYT-CF grant 263356), and by the German Research Foundation (DFG) as part of the Excellence Strategy of the federal and state governments – EXC 2094-390783311. We

are grateful to R. Neri for fruitful discussions. DJ was supported by National Research Council Canada (NRC) and by a Natural Sciences and Engineering Research Council of Canada (NSERC Discovery Grant). GB acknowledges funding from the State Agency for Research (AEI) of the Spanish Ministerio de Ciencia, Innovación y Universidades (MCIU) through the PID2020-117710GB-I00 grant funded by The Spanish Ministry of Science and Innovation (MCIN/AEI/10.13039/501100011033). We thank the anonymous referee for the very constructive comments and suggestions.

DATA AVAILABILITY

The raw data will be available on the ALMA archive at the end of the proprietary period (ADS/JAO.ALMA#2018.1.01205.L).

REFERENCES

Akiyama E., 2019, AJ, 157, 165
Alves F. O., Caselli P., Girart J. M., Segura-Cox D., Franco G. A. P., Schmiedeke A., Zhao B., 2019, Science, 366, 90
Alves F. O., Cleeves L. I., Girart J. M., Zhu Z., Franco G. A. P., Zurlo A., Caselli P., 2020, ApJ, 904, L6
Andre P., Martin-Pintado J., Despois D., Montmerle T., 1990, A&A, 236, 180
Andre P., Ward-Thompson D., Barsony M., 1993, ApJ, 406, 122
Ansdell M. et al., 2016, ApJ, 828, 46
Bate M. R., 2018, MNRAS, 475, 5618
Beckwith S. V. W., Sargent A. I., Chini R. S., Guesten R., 1990, AJ, 99, 924
Bontemps S., Andre P., 1997, in Reipurth B., Bertout C., eds, from Infall to Outflow, Poster proceedings of IAU Symposium No. 182 on Herbig-Haro Objects and the Birth of Low Mass Stars., Herbig-Haro Flows and the Birth of Stars, Vol. 182. p. 63
Caratti o Garatti A., Giannini T., Nisini B., Lorenzetti D., 2006, A&A, 449, 1077
Chen X. et al., 2013, ApJ, 768, 110
Chen Y.-C., Hirano N., 2018, ApJ, 868, 80
Clarke C. J., Pringle J. E., 1993, MNRAS, 261, 190
Codella C. et al., 2022, MNRAS, 515, 543
Cornwell T. J., 2008, IEEE J. Sel. Top. Signal Process., 2, 793
Cuello N. et al., 2019, MNRAS, 483, 4114
Cuello N. et al., 2020, MNRAS, 491, 504
Cuello N., Ménard F., Price D. J., 2023, Eur. Phys. J. Plus, 138, 11
Dong R., 2022, Nat. Astron., 6, 331
Duchêne G., Bontemps S., Bouvier J., André P., Djupvik A. A., Ghez A. M., 2007, A&A, 476, 229
Gagné J. et al., 2018, ApJ, 856, 23
Garufi A. et al., 2022, A&A, 658, A104
Hara C. et al., 2021, ApJ, 912, 34
Harris R. J. et al., 2018, ApJ, 861, 91
Hildebrand R. H., 1983, QJRAS, 24, 267
Hsieh C.-H., Lai S.-P., Cheong P.-I., Ko C.-L., Li Z.-Y., Murillo N. M., 2020, ApJ, 894, 23
Hull C. L. H., Le Gouellec V. J. M., Girart J. M., Tobin J. J., Bourke T. L., 2020, ApJ, 892, 152
Jacobsen S. K. et al., 2018, A&A, 612, A72
Kawabe R. et al., 2018, ApJ, 866, 141
Liu H. B., 2016, Sci. Advan., 2, e1500875
Louvet F., Dougados C., Cabrit S., Mardones D., Ménard F., Tabone B., Pinte C., Dent W. R. F., 2018, A&A, 618, A120
Maury A., Ohashi N., André P., 2012, A&A, 539, A130
McMullin J. P., Waters B., Schiebel D., Young W., Golap K., 2007, in Shaw R. A., Hill F., Bell D. J., eds, ASP Conf. Ser. Vol. 376, Astronomical Data Analysis Software and Systems XVI. Astron. Soc. Pac., San Francisco, p. 127
Ménard F. et al., 2020, A&A, 639, L1
Michel A., Sadavoy S. I., Sheehan P. D., Looney L. W., Cox E. G., 2022, ApJ, 937, 104
Müller H. S. P., Schlöder F., Stutzki J., Winnewisser G., 2005, J. Mol. Struct., 742, 215
Murillo N. M., Harsono D., McClure M., Lai S. P., Hogerheijde M. R., 2018, A&A, 615, L14
Murillo N. M., Lai S.-P., 2013, ApJ, 764, L15
Murillo N. M., Lai S.-P., Bruderer S., Harsono D., van Dishoeck E. F., 2013, A&A, 560, A103
Murillo N. M., van Dishoeck E. F., Hacar A., Harsono D., Jørgensen J. K., 2022, A&A, 658, A53
Offner S. S. R., Moe M., Kratter K. M., Sadavoy S. I., Jensen E. L. N., Tobin J. J., 2022, preprint (arXiv:2203.10066)
Ohashi S. et al., 2022, ApJ, 927, 54
Pfalzner S., 2003, ApJ, 592, 986
Pineda J. E. et al., 2012, A&A, 544, L7
Pineda J. E. et al., 2015, Nature, 518, 213
Pineda J. E. et al., 2022, preprint (arXiv:2205.03935)
Pineda J. E., Segura-Cox D., Caselli P., Cunningham N., Zhao B., Schmiedeke A., Maureira M. J., Neri R., 2020, Nat. Astron., 4, 1158
Podio L. et al., 2020, A&A, 642, L7
Rau U., Cornwell T. J., 2011, A&A, 532, A71
Reipurth B., 2000, AJ, 120, 3177
Reipurth B., Mikkola S., 2012, Nature, 492, 221
Sadavoy S. I. et al., 2019, ApJS, 245, 2
Sadavoy S. I., Stahler S. W., 2017, MNRAS, 469, 3881
Santangelo G., Murillo N. M., Nisini B., Codella C., Bruderer S., Lai S. P., van Dishoeck E. F., 2015, A&A, 581, A91
Takakuwa S., Saigo K., Matsumoto T., Saito M., Lim J., Hanawa T., Yen H.-W., Ho P. T. P., 2017, ApJ, 837, 86
Teague R., Jankovic M. R., Haworth T. J., Qi C., Ilee J. D., 2020, MNRAS, 495, 451
Tobin J. J. et al., 2016, ApJ, 818, 73
Tobin J. J. et al., 2022, ApJ, 925, 39
Valdivia-Mena, 2022, A&A, 667, A12
van der Wiel M. H. D. et al., 2019, A&A, 626, A93
Ward-Thompson D., André P., Crutcher R., Johnstone D., Onishi T., Wilson C., 2007, in Reipurth B., Jewitt D., Keil K., eds, Protostars and Planets V. Univ. Arizona Press, Tucson, AZ, p. 33
Zamponi J., Maureira M. J., Liu H. B., Zhao B., Segura-Cox D., Ko C., Caselli P., submitted to A&A
Zamponi J., Maureira M. J., Zhao B., Liu H. B., Ilee J. D., Forgan D., Caselli P., 2021, MNRAS, 508, 2583
Zapata L. A., Rodríguez L. F., Fernández-López M., Palau A., Estalella R., Osorio M., Anglada G., Huelamo N., 2020, ApJ, 896, 132

APPENDIX A: CHANNEL MAPS OF $C^{18}O$ (2–1) TOWARDS SOURCE W AT LOW VELOCITIES

Fig. A1 shows the channel maps of $C^{18}O$ (2–1) emission towards source W at low velocities, i.e. up to ± 1.8 km s^{-1} with respect to the systemic velocity of W [V_{sys}(W) $\sim +1.6$ km s^{-1}]. The maps show that the kinematics of the gas in the disc, which is well detected at high velocities (see Fig. 3), is affected by the extended emission from the streamers and/or the residual envelope at low velocities.

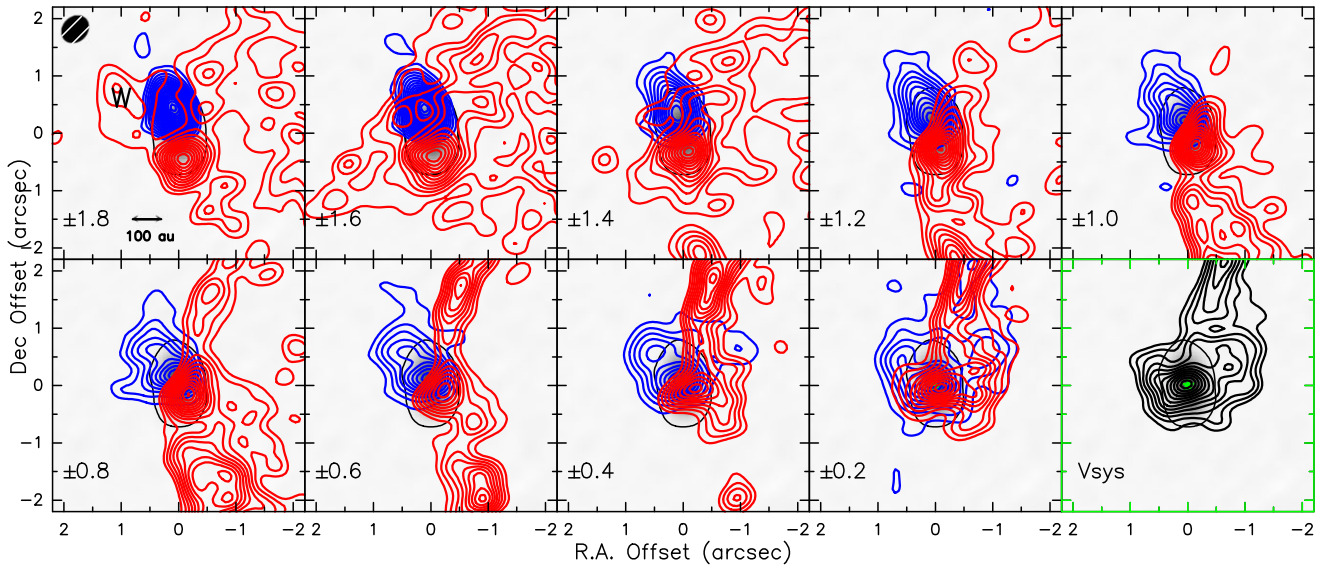

Figure A1. Channel maps of $C^{18}O$ (2–1) emission towards the VLA 1623W protostar (green star) at low redshifted and blueshifted velocities, i.e. up to ±1.8 km s^{-1} with respect to the VLA 1623W systemic velocity [V_{sys}(W) ∼ +1.6 km s^{-1}]. First contours and steps are 3σ (7.7 mJy per beam). The velocity offset with respect to V_{sys}(W) is reported in the bottom left corner of each panel. The black contour is the 3σ level of the 1.3 mm continuum emission, which is also shown by the greyscale background. The synthesized beam (0.48 arcsec × 0.40 arcsec) is shown in the top left corner of the first channel.

[1]*INAF, Osservatorio Astrofisico di Arcetri, Largo E. Fermi 5, I-50125 Firenze, Italy*
[2]*Dipartimento di Fisica e Astronomia, Universià degli Studi di Firenze, Via G. Sansone 1, I-50019 Sesto Fiorentino, Italy*
[3]*Univ. Grenoble Alpes, CNRS, IPAG, F-38000 Grenoble, France*
[4]*Institut de Radioastronomie Millimétrique, F-38406 Saint-Martin d'Hères, France*
[5]*École doctorale de Physique, Université Grenoble Alpes, 110 Rue de la Chimie, F-38400 Saint-Martin-d'Hères, France*
[6]*RIKEN Cluster for Pioneering Research, 2-1, Hirosawa, Wako-shi, Saitama 351-0198, Japan*
[7]*Instituto de Radioastronomía y Astrofísica, Universidad Nacional Autónoma de México, A.P. 3-72 (Xangari), 8701 Morelia, Mexico*
[8]*Instituto de Astronomía, Universidad Nacional Autónoma de México, Ciudad Universitaria, A.P. 70-264, 04510 Ciudad de México, Mexico*
[9]*NRC Herzberg Astronomy and Astrophysics, 5071 West Saanich Road, Victoria, BC V9E 2E7, Canada*
[10]*Department of Physics and Astronomy, University of Victoria, Elliott Building, 3800 Finnerty Road, Victoria, BC V8P 5C2, Canada*
[11]*Max-Planck-Institut für extraterrestrische Physik (MPE), Gießenbachstr 1, D-85741 Garching, Germany*
[12]*Department of Astronomy, The University of Tokyo, 7-3-1 Hongo, Bunkyo-ku, Tokyo 113-0033, Japan*
[13]*ORIGINS, Excellence Cluster Origins, Boltzmannstrasse 2, D-85748 Garching bei München, Germany*
[14]*Departament de Física Quàntica i Astrofísica, Universitat de Barcelona (UB), c/ Martí i Franquès 1, E-08028 Barcelona, Spain*
[15]*Institut de Ciències del Cosmos (ICCUB), Universitat de Barcelona, c. Martí i Franquès 1, E-08028 Barcelona, Spain*
[16]*Institut d'Estudis Espacials de Catalunya (IEEC), c. Gran Capità 2–4, E-08034 Barcelona, Spain*
[17]*Leiden Observatory, Leiden University, PO Box 9513, NL-2300 RA Leiden, the Netherlands*
[18]*European Southern Observatory, Karl-Schwarzschild-Strasse 2, D-85748 Garching bei München, Germany*
[19]*Department of Astronomy, University of Virginia, Charlottesville, VA 22904, USA*
[20]*National Radio Astronomy Observatory, PO Box O, Socorro, NM 87801, USA*
[21]*Centro de Astrobiología (CSIC/INTA), Ctra de Torrejón a Ajalvir km 4, E-28806 Torrejón de Ardoz, Spain*
[22]*Research Center for the Early Universe, The University of Tokyo, 7-3-1 Hongo, Bunkyo-ku, Tokyo 113-0033, Japan*

This paper has been typeset from a TEX/LATEX file prepared by the author.